# Automotive Engineering

Ludomir J. Jankowski, Ph.D. Eng.

## Testing of vehicle elements and assemblies

# Speckle photography in sandwich construction displacement measurements

Project co-financed by European Union within European Social Fund

# Introduction

The holography development was connected with the coherent speckle effect, which was firstly treated as a noise problem in a holographic image observation. The so-called "speckling" observed during an illumination of a rough object's surface with a coherent light is the basic phenomenon of the full-field, non contact displacement measurement technique.

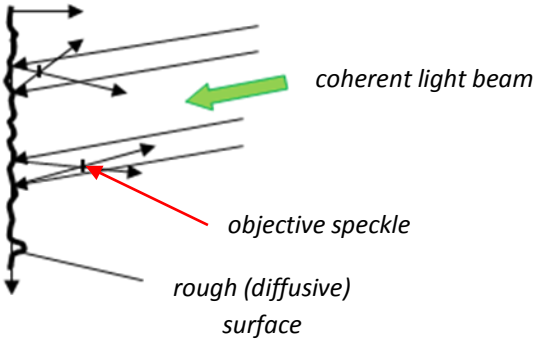


Fig. 1 Formation of the objective speckles by a diffusive object

The random interference of the coherent light rays reflected from the diffusive surface (fig. 1) produces objective speckle patterns formed in the whole space in front of the object. This random field distribution of speckles is stationary in time and is a function of the spatial coordinates. When the illuminated surface is projected by an optical system (camera lens, human eye) on any "screen", the resultant speckle patterns are called subjective (because they are transformed by the system) – fig. 2.

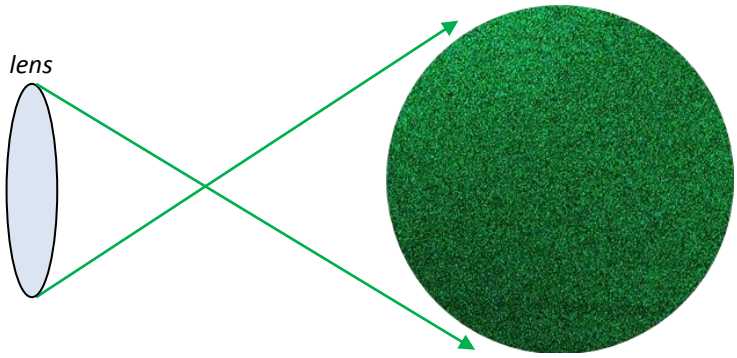


Fig. 2 The subjective speckle patterns

The size of these speckles depends only on the angular extent of the image by the optical system. For example, if camera lens is used for recording of the image of the coherent light illuminated surface, the speckle average size (treated as a circular diaphragm or a hole) is a function of the angular size of the lens aperture. This inversely proportional relation is given by:

$$\sigma \cong 1.2\lambda F = 1.22\lambda \frac{L}{D} \qquad (1)$$

where: $F$ – the number of the lens
$L$ – distance between image and object
$D$ – aperture of the lens
$\lambda$ – light wavelength

The probability density function of speckle intensity variations at the image plane is determined by:

$$p(I) = \frac{1}{I_0} exp\left[-\left(\frac{I}{I_0}\right)\right] \qquad I > 0$$

$$p(I) = 0 \qquad I \leq 0 \tag{2}$$

Thus the most probable intensity of the speckle is zero (dark speckle) – fig. 3.

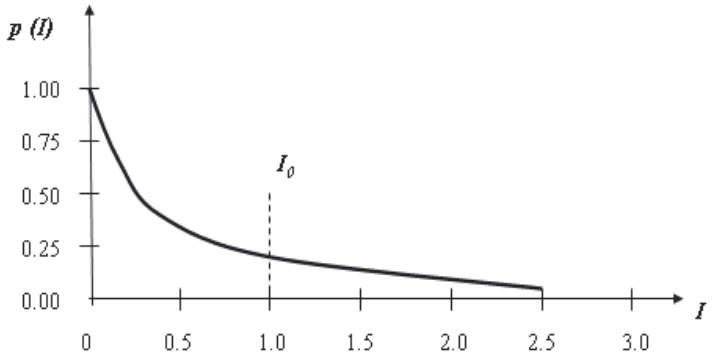


Fig. 3 Distribution of the light intensity in the speckle field

It must be noted that the speckle pattern is a result of the interference, but the speckle photography method is based on the incoherent mechanism and the phase information about the object's surface is not exploited. Generally, the speckle photography technique's sensitivity is less then interferometric methods (classical interferometry, holographic interferometry). It is often an advantage because lesser restrictions for measurement conditions are required.

# Speckle photography techniques

## ➢ *in-plane displacement measurement*

The speckle photography method (in coherent light) utilizes the correlation between a surface point and the subjective speckle pattern. The tested object is illuminated with an expanded laser beam and in front of the object's surface a coherent speckle pattern appears. This image is projected by an optical system on the photosensitive plate (as a rule holographic materials are used because the high resolution of the emulsion is needed). So the subjective speckle pattern corresponding to the "first" object's surface stage is registered. Then the object is deformed or translated in the space and the "second" subjective speckle pattern is captured on the same photosensitive plate. Practically, the double-exposed specklegram is a negative image of the object covered by two speckle patterns systems. The displacement between the speckles generated by the surface small area (assumed as a point) is registered on the specklegram accordingly to the loading increasing between expositions. The relationship between the in-plane displacement vector of the deformed object and speckle displacement in the image plane (on the specklegram) is:

$$\vec{d} = \frac{\vec{s}}{M} \tag{3}$$

where: $\vec{d}$ - in-plane displacement vector of the object point

$M$ – photographic magnification

$\vec{s}$ - displacement vector of the speckles (in specklegram plane)

The obtained specklegram is analysed using the point-by-point or full-field technique for determining the in-plane displacement value. In the first case, a coherent light beam with a small diameter is passing through the specklegram and the optical Fourier transformation occurs – the light rays diffracted on the two speckle families generate two displaced wavefronts. At the distance *L* from the specklegram the parallel fringes with a constant fringe spacing appear – fig. 4.

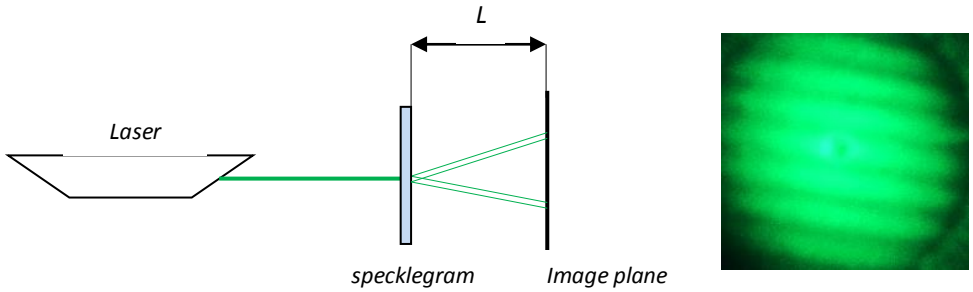


Fig. 4 Scheme of the point-by-point specklegram analysis (filtering)

This well known effect (classical Young's experiment) is generated by several pairs of the illuminated speckles with similar orientation and spacing. The in-plane displacement vector value is determined by equation:

$$|\vec{d}| = \frac{\lambda\sqrt{4L^2 + a^2}}{2Ma} \tag{4}$$

where: *a* – fringe spacing

Practically, $4L^2 \gg a^2$ is common and eq. (4) is:

$$|\vec{d}| = \frac{\lambda L}{Ma} \tag{5}$$

The in-plane displacement direction is perpendicular to the fringe direction – fig. 5 - and the in-plane components (*u* – along x axis, *v* – along y axis) can be calculated using the following relationships:

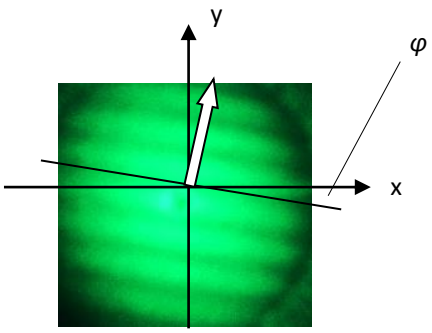


Fig. 5 Coordinate system for in-plane displacement vector components calculation

$$u = |\vec{d}| \sin\varphi = \frac{\lambda L}{Ma} \sin\varphi \tag{6}$$

$$v = |\vec{d}| \cos\varphi = \frac{\lambda L}{Ma} \cos\varphi$$

The full-field method of the specklegram analysis is based on the Fourier filtering technique. The optical arrangement for this filtering is presented in fig. 6.

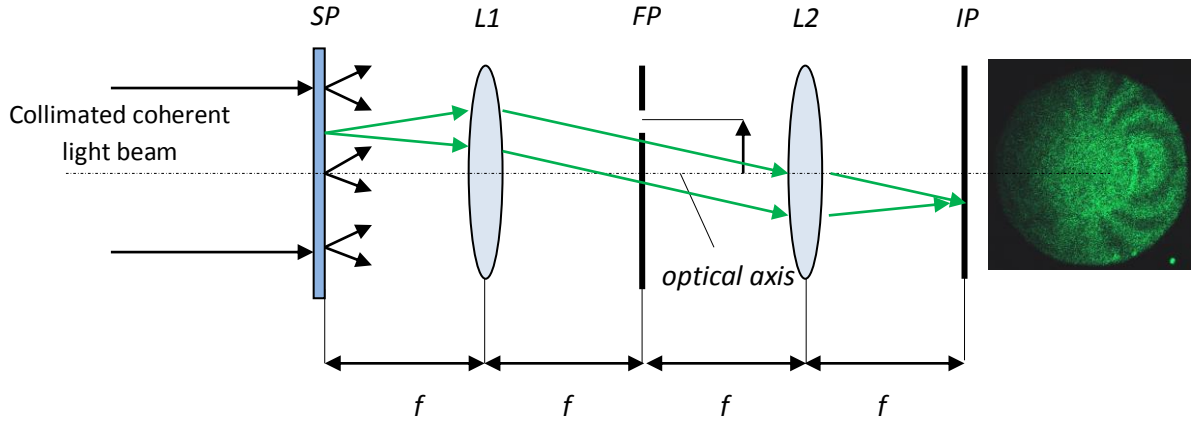


Fig. 6 A Fourier filtering arrangement for full-field specklegram analysis

The specklegram with a large number of speckle pairs is placed in the plane **SP**. It acts as a diffraction grid. Each pair of speckles forms diffracted rays at the angles which are given by a diffraction equation:

$$s_s \sin\alpha = N\lambda \tag{7}$$

where: $s_s$ – distance between centres of the speckles (circular apertures) forming the pair
$\alpha$ – diffraction angle
$N$ – order of diffraction
$\lambda$ – wavelength of the light used for analysis

The orientation of the speckle pair determines the angle in the Fourier plane (***FP***) at which the diffracted light appears. Through a small aperture in the diaphragm, placed off-axis in the ***FP*** plane, only the light diffracted from the pairs of speckles of a particular separation (or a multiple of that spacing) with a particular orientation passes. Then the lens ***L2*** forms in the ***IP*** plane the image of the object covered by the fringes. These fringes are connected with the in-plane displacement component oriented along the line joining the centre of the aperture and the optical axis of the filtering set-up. By varying the filtering aperture position, displacement components in any direction can be extracted from the specklegram. Practically, by placing the aperture on the coordinate system axes, the components *u* and *v* can be determined using the equations:

$$u = N_x \lambda \frac{f}{q_x M}; \qquad v = N_y \lambda \frac{f}{q_y M} \tag{8}$$

where: $N_x$, $N_y$ – fringe order determined for aperture location on *x(y)* axis
$q_x$, $q_y$ – distance of the aperture centre from the optical axis
$f$ – focal length

The magnitude of the vector *d* is:

$$|\vec{d}| = \frac{\lambda f}{M}\sqrt{\left(\frac{N_x}{q_x}\right)^2 + \left(\frac{N_y}{q_y}\right)^2} \tag{9}$$

and direction is:

$$\alpha_{dv} = arctan\frac{v}{u} = arctan\frac{N_y q_x}{N_x q_y} \tag{10}$$

The speckle photography is limited by the nature of the phenomenon causing the diffraction of the light on the speckle pairs registered on the specklegram. The displacement between the first and the second exposure must be greater than the distance between centres of the speckles – fig. 7.

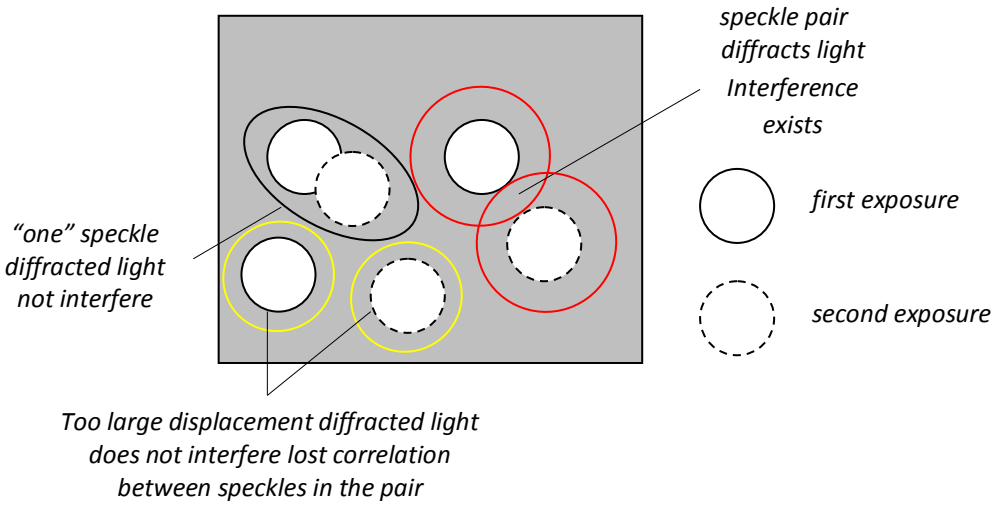


Fig. 7 Limitation of the displacement value measurement

The measurement lower limit is the function of the speckle average size, i.e. speckle registration process determines the minimal value of the displacement *d*:

$$|\vec{d}| \geq \frac{1.22\lambda F}{M} \tag{11}$$

The limit (11) may be omitted by an addition of the known (value and direction) displacement of the object (treated as a rigid body) between the first and the second exposure.

The upper limit of the measurement is connected with the possibility of the diffraction mechanism existing. Too large a distance between the centres of the speckles in the pair causes the absence of the conditions suitable for a diffracted light interference.

## ➢ *out-of-plane displacement measurement*

Some authors refer to speckle photography as insensitive to the out-of-plane displacements but it is evident that the speckle can be used for such measurements too. It was previously signalized that speckles are formed in the space in front of the object's rough surface. This surface is illuminated by a collimated beam of the coherent light inclined at an angle *Θ* to the recording system axis. The speckle structure is imaged by recording lens ***RL*** with the maximal aperture on the

photosensitive plate ***SP*** placed at a distance c from the image plane ***IP*** – fig. 8. Displacements of the speckles lying in this plane are correlated with the angle of normal to the surface rotation. Tangent of this angle is:

$$\tan\varphi = \frac{|\vec{s}|}{2Mc}; \qquad \tan\varphi = \frac{\partial w}{\partial x_k} \tag{12}$$

In equations (12) the variable *w* is the deflection of the surface and $x_k$ is the direction of the derivative calculation.

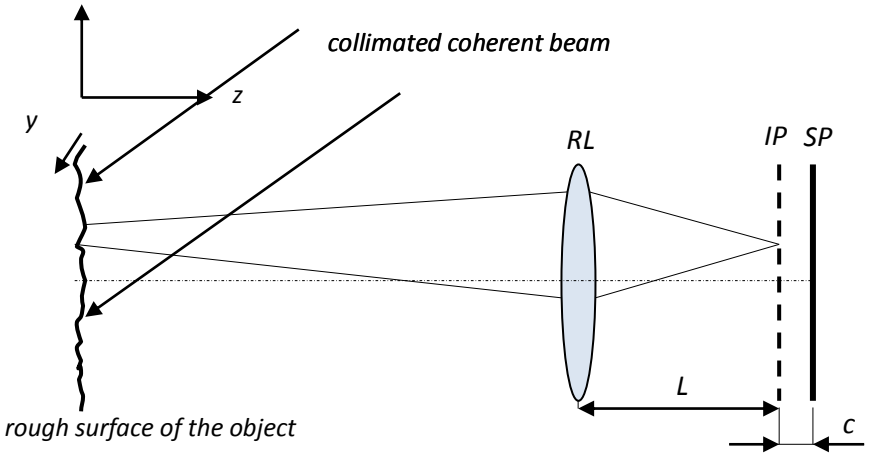


Fig. 8 Scheme of the specklegram recording for out-of-plane displacement measurement

The recorded specklegram is analyzed using the point-by-point technique and the derivative is:

$$\frac{\partial w}{\partial x_k} = \lambda\frac{\sqrt{4L^2 + a^2}}{4Mac} \cong \frac{\lambda L}{2Mac} \tag{13}$$

Using Fourier filtering scheme, the derivatives for *x* and *y* direction are:

$$\frac{\partial w}{\partial x} = \frac{N_x\lambda\sqrt{f^2 + q_x^2}}{4Mcq_x} \cong \frac{N_x\lambda f}{4Mcq_x}; \qquad q_x^2 \ll f^2$$

$$\frac{\partial w}{\partial y} = \frac{N_y\lambda\sqrt{f^2 + q_y^2}}{4Mcq_y} \cong \frac{N_y\lambda f}{4Mcq_y}; \qquad q_y^2 \ll f^2 \tag{14}$$

The deflection *w* may be determined by integration. For example, the first equation (14) yields:

$$w = \int dw = \frac{\lambda f}{4Mcq_x}\int N_x(x)\,dx \tag{15}$$

An advantage of the Fourier filtering is the possibility to dense the information about *N* on the whole observed surface by placing (from the optical axis) the aperture in several positions.

As an example of the "multiplication" data by analysis specklegram at different offset, the series of the images registered for deflection measurement of a circular plate (restrained on the radius *a* with a central hole with diameter *2r*) is presented. The plate was loaded uniformly with pressure *q* – fig. 9. The fringes images for different offset ($q_{x1} < q_{x2} < q_{x3} < q_{x4} < q_{x5}$) are shown in fig. 10.

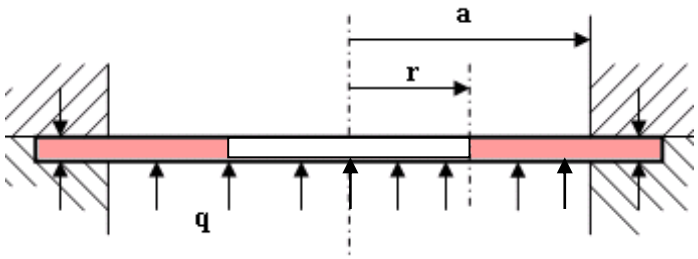


Fig. 9 Scheme of the plate loading

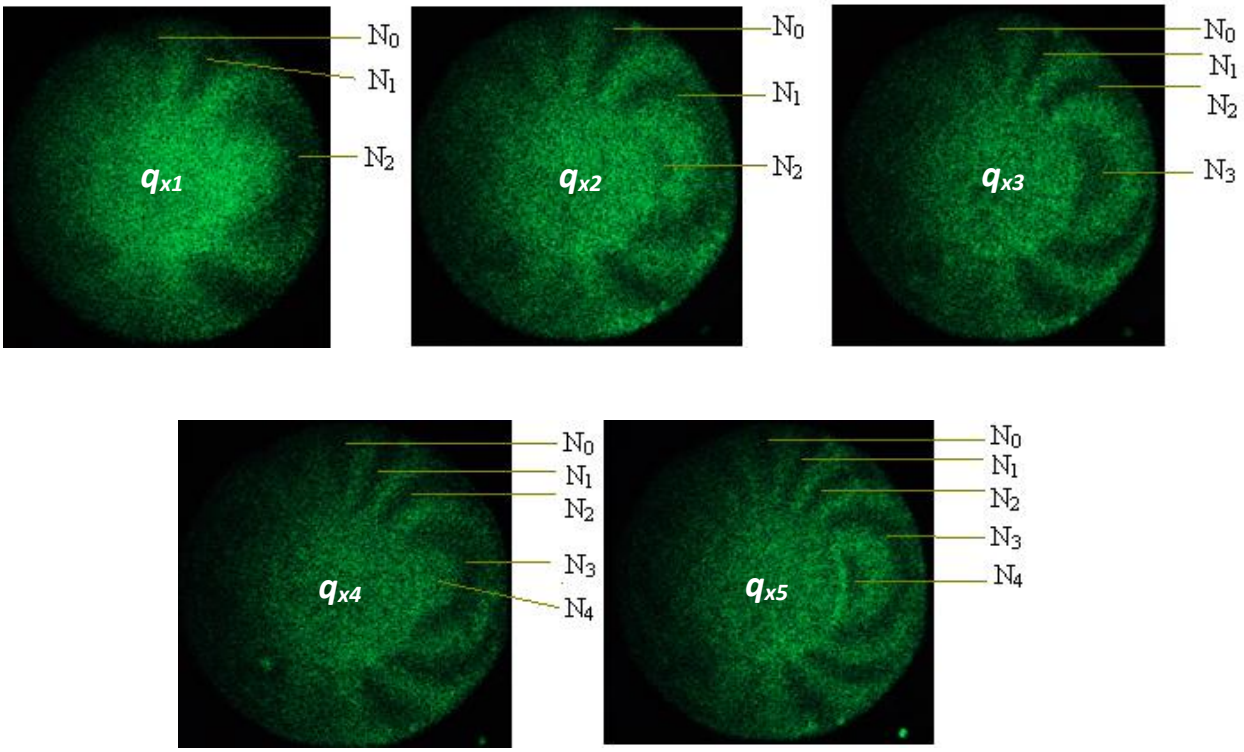


Fig. 10 Images of the fringes observed at different offset $q_x$
($q_{x1}$ = 30 mm, $q_{x2}$ = 35 mm, $q_{x3}$ = 40 mm, $q_{x4}$ = 45 mm, $q_{x5}$ = 50 mm)

# Sandwich constructions

The term "sandwich construction" is used for an element consisting of two relatively thin, dense, high strength and parallel sheets of structural material (steel, aluminium, composites) with their faces bonded to and separated by a relatively thick, light weight core such as metallic and non-metallic honeycombs, cellular foams like foamed plastics,

balsa wood or trusses. Thanks to the bonding of the core to the facings with proper adhesives, they can act as a composite load-bearing unit with a characteristic distribution of load capacity. The facings carry almost all of the in-plane or bending stresses and the core acts as a support of the facings and carries the shear stresses. The high stiffness of the sandwich construction is an effect of the facings separation, which increases the moment of inertia of the unit (fig. 11). The mechanical properties of sandwich structures are a function of their geometry, loading scheme, level of the load, properties of the facings, core and adhesive materials. Sandwich constructions are used widely in space, aircraft, automotive and civil engineering.

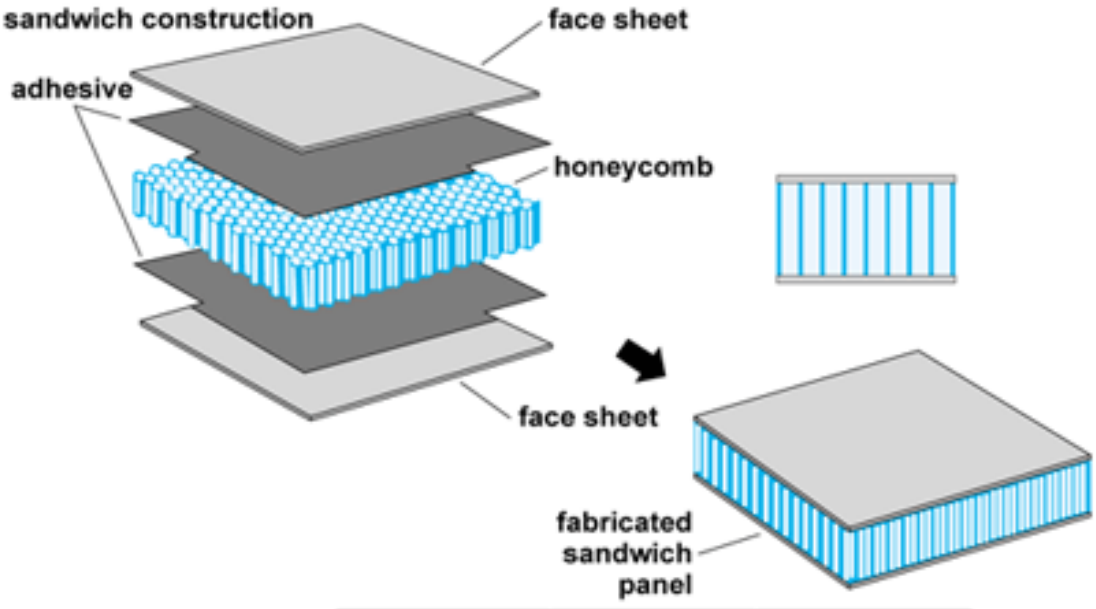


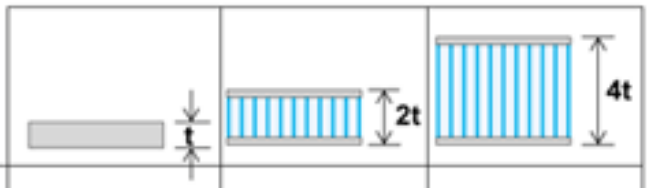


| | | | |
|---|---|---|---|
| Relative stiffness (D) | 100 | 700 | 3700 |
| Relative strength | 100 | 350 | 925 |
| Relative weight | 100 | 103 | 106 |

Fig. 11 An example of honeycomb plate construction and table of the relative properties at constant summary thickness of the faces

The thin facings are used to carry loads in a sandwich and prevention of local failure under edgewise direct or flat wise bending loads is necessary. Modes of failure that may occur in a sandwich under edge compression load are shown in fig. 12. An example of the local failure caused by loading acting perpendicularly to the facing is presented in fig. 13.

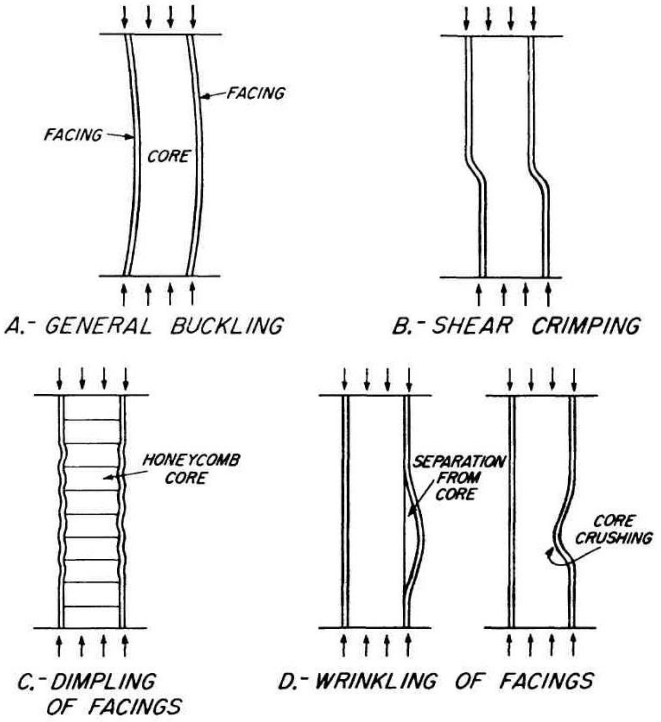


Fig. 12 Modes of the compressed sandwich construction failure

Fig. 13 An effect of the pointwise loading of the sandwich structure without reinforcement (aluminum facings, polyurethane foam core)

The stiffness of the sandwich composites is an important parameter which shows (together with weight determination) the efficiency of application of these structures. For example, the sandwich beam with a rectangular cross-section (fig. 14) and equal thickness of the facings, made from homogeniuous, isotropic material under normal forces has the bending stiffness of:

$$D_b = D + 2D_f = \frac{bE_f t_f}{2}\left[\left(h_c + t_f\right)^2 + \frac{t_f^2}{3}\right] \tag{16}$$

If the beam is tensioned or compressed in the facings planes the stiffness is:

$$A_t = \left(2E_f t_f + E_c h_c\right)b \tag{17}$$

For a beam with thin facings and a thick core, the transverse shear stiffness is:

$$S \cong h_c b G_c \tag{18}$$

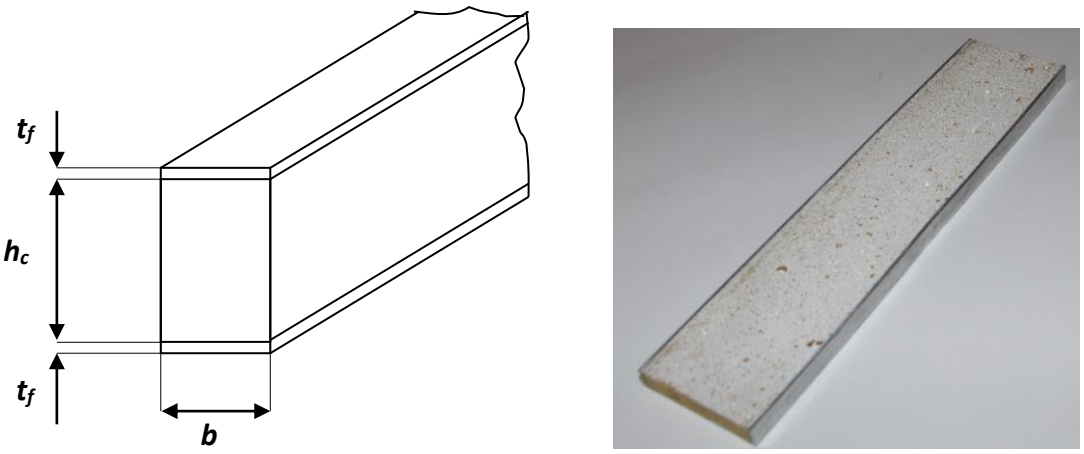


Fig. 14 Notation for stiffness calculations

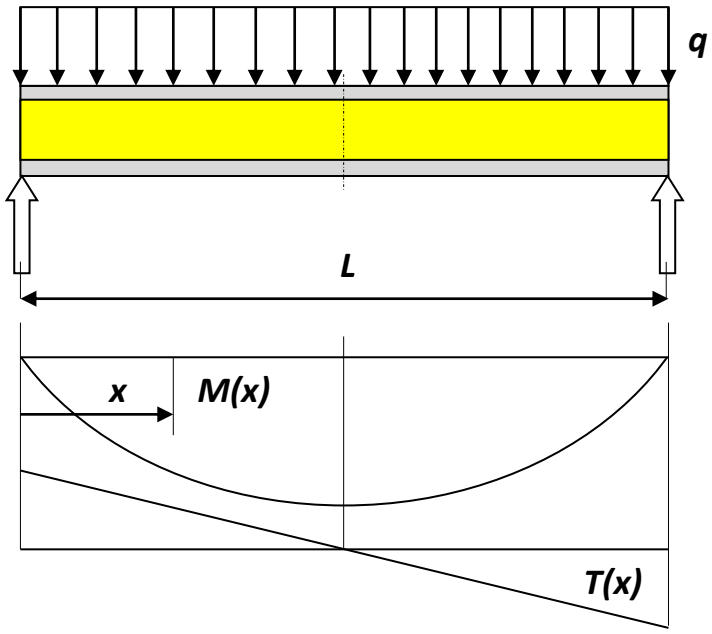


Fig.15 Scheme of the sandwich beam loading

Calculaction of the stresses is based on the well-known strength relations. For example, determination of the stresses for a sandwich beam with a constant cross-section (fig. 14), loaded uniformly, is presented above (fig. 15). The bending moment distribution *M(x)* and transverse force *T(x)* are distributed according to the relations:

$$M(x) = \frac{qL}{2}x - \frac{qx^2}{2}; \qquad M_{max} = q\frac{L^2}{8} \tag{18}$$

$$T(x) = -qx; \qquad T_{max} = -q\frac{L}{2} \tag{19}$$

The bending moment causes normal forces $N_f$ to act in plane of the facings according to the equation:

$$N_f = \frac{M}{(h_c + t_f)} \tag{20}$$

Thus normal stresses in the facings are:

$$\sigma_f = \frac{N_f}{t_f b} = \frac{M}{(h_c + t_f)t_f b} \tag{21}$$

and shear stresses in the core amount to:

$$\tau_c = \frac{T}{h_c b} \tag{22}$$

At the facing-core interface the compatibility strain equation is valid and in the core compressive or tensile stress occurs:

$$\sigma_c \cong \frac{M}{b t_f h_c}\left(\frac{E_c}{E_f}\right) \tag{23}$$

The compression face may be wrinkling, i.e. subjected to the short-wave buckling at the critical value of the compression forces acting in-plane of the facing. The critical wrinkling stress is studied for the compression of the thin plate (facing) supported on the core as an elastic continuum. For bending, this critical stress is expressed by:

$$\sigma_{bcr} = \sqrt{\left[\frac{2t_f}{3h_c}\frac{E_{c3}E_{f1}}{(1 - \nu_{c13}\nu_{c31})}\right]} \tag{24}$$

where $E_{c3}$ is the elastic modulus of the core in the direction *(3)* perpendicular to the facing plane and $\nu_{c13}$ ($\nu_{c31}$) are the Poisson ratio of the core material in plane determined by the loading direction *(1)* and the strain acting in *(3)*-direction.

For simultaneous bending and shear forces loading of the sandwich beam, the critical value of the wrinkling stress is:

$$\sigma_{cr}^{*} = c\left(\sqrt[3]{E_{f1}E_{c3}G_{c13}}\right) \tag{25}$$

The coefficient $c$ takes the values 0.5, 0.6 or 0.65 and $G_{c13}$ is the transverse shear modulus of the core. An analysis of the equations (24) and (25) shows the great role of the core material properties for facings wrinkling phenomenon appearance which is a common failure mode for bending or compression of sandwich beams. Higher values of the core elastic module ($E_{c3}$ and $G_{c13}$) in the transverse direction cause increasing of the wrinkling critical stresses. Additionally, the indentation resistance of the facing increases.

Deflection of the beam presented in fig. 15 is:

$$w = \frac{1}{D_b}\left[\frac{qL}{4}\frac{x^3}{3} - q\frac{x^4}{24}\right] + \frac{q}{S}\frac{x^2}{2} - \frac{1}{D_b}\frac{qL^3}{24}x - \frac{qL}{2S}x \tag{26}$$

The maximum value of the deflection (for $x = L/2$) can be calculated as:

$$f = -\frac{1}{D_b}\frac{5}{384}qL^4 - q\frac{L^2}{8S} \tag{27}$$

The sandwich constructions designing criteria are firstly suitable for plane or straight elements but in real solutions often corners and curvatures exist. Below, a case of a curved sandwich beam under bending is presented. The curvature of the sandwich beam causes different (against straight beam) interaction between facings and core because transverse forces must act on the core in the transverse direction. Thus tensile or compressive strengths of the core and facings are critical criteria for a curved sandwich beam. The commonly used assumptions are taken to considerate the bending case:

- the stresses are only a function of radius
- so-called end effects are not considered
- materials are linear elastic isotropic or orthotropic
- the facings and core are bonded exactly
- plane stress or strain state in the layers formed beam is assumed

The definition of the geometrical parameters of a curved sandwich beam in pure bending is presented in fig. 16.

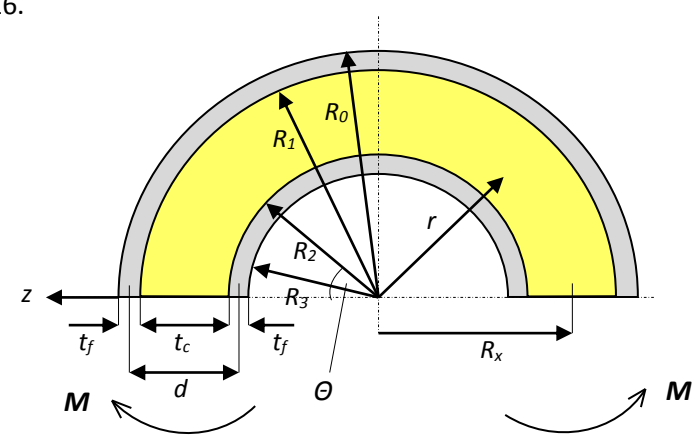


Fig. 16 Definition of the curved sandwich beam geometry

Two cases of the face thickness assumptions may be applied. The first one is a thin face approximation which leads to in-plane stresses in the facings:

$$\sigma_f(z) = \pm\frac{M}{t_f d}; \qquad \sigma_c(z) = 0 \tag{28}$$

where: $M$ is the bending moment per unit width.

The second case is a thick face approximation which leads to in-plane stresses:

$$\sigma_f = \frac{MzE_f}{D}, \qquad \frac{t_c}{2} < |z| \leq \frac{t_c}{2} + t_f \tag{29}$$

$$\sigma_c = \frac{MzE_c}{D}, \qquad -\frac{t_c}{2} < z \leq \frac{t_c}{2} \tag{30}$$

and bending stiffness is:

$$D = 2D_f + D_c + D_0 = E_f\left(\frac{t_f^3}{6} + \frac{t_f d^2}{2}\right) + E_c\frac{dt_c^2}{12} \tag{31}$$

The stresses in radial direction can be calculated as:

$$\sigma_r = \frac{M}{(R_x + z)d}, \qquad -\frac{t_c}{2} < z \leq \frac{t_c}{2} \tag{32}$$

The equations presented above are useful, for example, in calculation of the walls in a cylindrical tank loaded with inner pressure.

# Practical exercises

During practical exercises the following activities will be carried out:

- presentation of practical information about the technology of sandwich construction preparation,
- set up of the optical system for a double-exposure specklegram registration
- performance of the specklegram registration
- set up of the optical system for point-by-point or/and Fourier filtering analysis and making the measurement (data collection)
- determination of the displacements in the cross-section of the sandwich beam based on experimental measurement and stress calculation using the formulas presented above
- preparation of a report (its range will be determined by the lecturer).

## *References*

[1] Erf R.K.(ed.), Speckle Metrology, Academic Press, Inc., 1978
[2] Shelton J.C., Orr J.F., Optical Measurement Methods in Biomechanics, Chapman & Hall, 1997
[3] Allen H.G., Analysis and design of structural sandwich panels
[4] Falzon B.G., Aliabadi M.H., Buckling and Postbuckling Structures, Imperial College Press, 2008
[5] Smidt S., Bending of curved sandwich beams, Composite Structures, 33, 1995
[6] Gasvik K.J., Optical Metrology, III$^{rd}$ ed., John Wiley&Sons, Ltd., Chichester, England, 2002